A critical concentration of N-terminal pyroglutamylated amyloid beta drives the misfolding of Ab1-42 into more toxic aggregates

Denise Galante [a, e], Francesco Simone Ruggeri [b, c], Giovanni Dietler [b], Francesca Pellistri [d], Elena Gatta [d], Alessandro Corsaro [e], Tullio Florio [e], Angelo Perico [a], Cristina D'Arrigo, [a, *]

[a] *Institute for Macromolecular Studies, National Research Council, 16149 Genova, Italy*
[b] *Ecole Polytechnique Federale de Lausanne (EPLF), 1015 Lausanne, Switzerland*
[c] *Department of Chemistry, University of Cambridge, CB21EW, United Kingdom*
[d] *Department of Physics, University of Genova, 16100 Genova, Italy*
[e] *Section of Pharmacology, Department of Internal Medicine and Centre of Excellence for Biomedical Research (CEBR), University of Genova, 16132 Genova, Italy*

ARTICLE INFO

ABSTRACT

A wide consensus based on robust experimental evidence indicates pyroglutamylated amyloid-β isoform (AβpE3-42) as one of the most neurotoxic peptides involved in the onset of Alzheimer's disease. Furthermore, AβpE3-42 co-oligomerized with excess of Aβ1-42, produces oligomers and aggregates that are structurally distinct and far more cytotoxic than those made from Aβ1-42 alone. Here, we investigate quantitatively the influence of AβpE3-42 on biophysical properties and biological activity of Aβ1-42. We tested different ratios of AβpE3-42/Aβ1-42 mixtures finding a correlation between the biological activity and the structural conformation and morphology of the analyzed mixtures. We find that a mixture containing 5% AβpE3-42, induces the highest disruption of intracellular calcium homeostasis and the highest neuronal toxicity. These data correlate to an high content of relaxed antiparallel β-sheet structure and the coexistence of a population of big spheroidal aggregates together with short fibrils. Our experiments provide also evidence that AβpE3-42 causes template-induced misfolding of Aβ1-42 at ratios below 33%. This means that there exists a critical concentration required to have seeding on Aβ1-42 aggregation, above this threshold, the seed effect is not possible anymore and AβpE3-42 controls the total aggregation kinetics.

© 2016 Published by Elsevier Ltd.

1. Introduction

Alzheimer's disease (AD), the most common form of dementia with a high incidence in the population over 65, is estimated to globally affect 1 out of 85 people by 2050 (Brookmeyer et al., 1998, 2007). Extracellular plaques of amyloid-β (Aβ) peptides and intraneuronal neurofibrillary tangles, made from tau hyperphosphorylation, are the main histopathological signatures of AD (Tanzi, 2005; Nussbaum et al., 2012). Aβ peptides are the major components of AD plaques and consist a mixture of peptides having different N and C-termini (Russo et al., 2000). In the last fifteen years, it has been suggested that despite the importance of plaques to AD pathology, soluble Aβ oligomers are the principal toxic forms of Aβ (Kirkitadze et al., 2002; Walsh et al., 2002). The Aβ peptide family is produced by sequential endoproteolytic processing of the amyloid precursor protein (APP) by β-and γ-secretases. Cleavage by γ-secretase at different sites primarily results in Aβ1-40 and Aβ1-42 species that differ at their C-termini. N-terminal heterogeneity is caused by alternative cleavage of APP by β-secretase. Among these, 15–20% are N-terminus pyroglutamylated (pE), catalysed by glutaminyl cyclase (Schilling et al., 2008). The most abundant pyroglutamylated species *in vivo* is AβpE3-42 (Tabaton et al., 1994). N-terminally truncated and *pyro*-modified Aβ peptides show faster aggregation kinetics than full-length β-peptides (D'Arrigo et al., 2009; Schilling et al., 2006). The structural modifications in AβpE3-42 change the attitude of the full-length Aβ1-42 from a slow to a faster aggregation process (Perico et al., 2011). Literature data, about the pattern of fibrillogenesis of AβpE and unmodified peptides are often conflicting, because of the inherent polymorphism of the peptides and the experimental conditions adopted (Petkova et al., 2005; Jeong et al., 2013). A detailed characterization of the oligomeric and prefibrillar states, allowed the discrimination of the intermediate states mainly responsible of oligomer toxicity, confirming the peculiar role of AβpE3-42 in the pathogenesis of AD (Galante et al., 2012). In 1995, by examination of cortical sections from AD patients, it was found that AβpE3-x peptides were present in equivalent or greater densities than full length peptides (Saido et al., 1995). Subsequently, the neurotoxic effect of oligomers was related to the predominance of AβpE3-42 (Russo et al., 2002). However, the relative abundances of AβpE and unmodified peptides remain controversial. While several reports indicate that AβpE3-x is more abundant than Aβ1-x in AD (Frost et al., 2013),

* Corresponding author at: Institute for Macromolecular Studies, National Research Council, Via De Marini 6, 16149 Genova, Italy.
Email address: cristina.darrigo@ge.ismac.cnr.it (C. D'Arrigo).

others reported that the two species were in similar concentrations (Moore et al., 2012) and in advance stage AD (Wu et al., 2014). By the contrast, Pivtoraiko et al. (2015) found in posterior cingulated cortex same concentrations for AβpE3-x and Aβ1-x in insoluble pool but only for Aβ1-42 in soluble pool. Low concentrations of soluble AβpE3-x reflect its rapid aggregation into plaques. Upadhaya et al. (2014) demonstrated that AβpE are not only detectable in the plaques but also in soluble and dispersible Aβ aggregates outside of the plaques. Biophysical studies showed that mixtures of the two peptides (*pyro*-modified/truncated and unmodified Aβ) cause an initial delay in β-sheet formation from both equimolar and no-equimolar samples, concluding that AβpE3-42 affects early aggregation process of unmodified peptides (Sanders et al., 2009). A tight interaction between AβpE3-42 and the unmodified peptide was showed by Fourier Transform Infrared Spectroscopy (FTIR) experiments, demonstrating that AβpE3-42, in 10% and 50% mixtures, transmits specific structural features to Aβ1–42 by a prion-like mechanism (Matos et al., 2014). These data leave the open question of which are the amounts of AβpE3-42 that have a sensitive influence on the biological activity, aggregation kinetics, secondary structure, and morphology of Aβ1-42. Is there a correlation between biological activity and structure or morphology? How does the structure of the mixed aggregates change, compared to the structure of the unmodified, Aβ1-42, aggregates?

In this manuscript we compare the biological activity, aggregation kinetics, conformational behavior, structure and morphology of mixtures of the Aβ1-42 and AβpE3-42 peptides, from 2.5% to 50% of AβpE3-42, to those of the two peptides alone. The biological activity is evaluated by measuring the variations of intracellular calcium concentrations, and by *in vitro* neurotoxicity, evaluating cell viability. The secondary structure is analysed by circular dichroism (CD) and by infrared nanospectroscopy (NanoIR). The aggregation is followed by turbidity experiments. Finally, the morphology of the aggregates is obtained by Atomic Force Microscopy (AFM) and Transmission Electron Microscopy (TEM).

2. Materials and methods

2.1. Aβ sample preparation

One milliliter of dimethyl sulfoxide (DMSO; Sigma) was added to 1 mg of lyophilized synthetic peptide (Aβ1-42 or AβpE3-42; AnaSpec), reaching a final concentration of 1 mg/ml. Aliquots of 75 μl were lyophilized and stored at −20 °C until used. For all experiments, stock peptides were reconstituted as reported Galante et al. (2012). The concentration of the peptide was estimated using a molar extinction coefficient at 214 nm, by Shimadzu UV 2700 Spectrophotometer (Hung et al., 2008). For the preparation of the mixtures, Aβ1-42 and AβpE3-42 were first mixed in microfuge tubes at different concentration ratios and diluted at 10 μM of total peptides concentration in Phosphate Buffered Saline (PBS, 150 mM, pH 7.4). pH of mixtures was corrected at 7.4 with few μl of 1 M HCl. Using these peptide solutions, we prepared mixtures at 2.5%, 5%, 10%, 20%, 33%, 50%, in which the percentage indicates the amount of AβpE3-42 over the total concentration of peptides.

2.2. Neurons preparation and Aβ treatments

Cerebellar granule cells were prepared from Sprague–Dawley rats (Harlan, Bresso, Italy). Experimental procedures and animal care complied with the EU Parliament and Governing Council of 22 September 2010 (2010/63/EU) and were approved by the Italian Ministry of

Health (protocol number 2207) in accordance with D.M. 116/1992. All efforts were made to minimize animal suffering and to use the minimum number of animals necessary to produce reliable results. Granule cells were prepared from cerebella of 7–8 day old rats following the procedure of Levi et al. (1984) as previously described (Robello et al., 1993). Cells were plated at 1×10^6 per dish on 20 mm poly-L-lysine-coated glass coverslips and maintained in Basal Eagle's culture medium, containing 10% fetal calf serum, 100 μg/ml gentamicin and 25 mM KCl, at 37 °C in a humidified 95% air, 5% CO_2 atmosphere. Cultures were treated with 10 μM cytosine arabinoside since the first day in order to minimize proliferation of non-neuronal cells. In a range of time between 6 and 12 days after plating, cells were treated for 20 h with Aβ peptides alone and mixtures (1 μM), which were oligomerized for 24 h at 37 °C at the concentration of 10 μM before dilution into culture media. Then, the intracellular free Ca^{2+} concentrations increase, was measured in the cells by means of the fluorescent probe Oregon Green.

2.3. Intracellular Ca^{2+} concentration measurements by oregon green fluorescence

Following Aβ treatments, neurons were incubated at 37 °C for 40 min in a 6.0 μM solution of the cell-permeant AM ester of Oregon Green (Molecular Probes, Eugene, OR) and then washed several times with washing solution (135 mM NaCl, 5.4 mM KCl, 1.8 mM $CaCl_2$, 1.0 mM $MgCl_2$, 5.0 mM Hepes, 10 mM glucose, pH 7.4). Then cultures were transferred to a recording chamber mounted onto a Nikon Eclipse TE300 inverted microscope. Cells were visualized using a ×100 objective in oil (N.A. 1.3) as previously described (Pellistri et al., 2008). The fluorescence signal was detected using a Hamamatsu digital CCD camera with a 450–490 nm excitation filter, a 505 nm dichroic mirror, and a 520 nm emission filter (Nikon Italia, Florence, Italy). Images were acquired with the Simple PCI software (Hamamatsu, Sewickley, PA). Fluorescence intensity was calculated in arbitrary units by building a scale of the pixel intensity located in the region of interest. Fluorescence intensity changes were calculated as $(F − F_0) \times 100/F_0$, where F was the fluorescence intensity measured after Aβ treatment and F_0 the basal fluorescence level. Three independent experiments in duplicate were done. For each replicate the fluorescence of at least 40 cells was analyzed to obtain an average of the signal. Statistical analysis was performed by means of one-way ANOVA using "Newman-Keuls multiple comparison post-hoc test".

2.4. A1 neuron cultures and Aβ treatment

Neuronal Mes-c-myc A1 (hereafter A1) cell line was generated by immortalization of primary cultures of mouse embryonic mesencephalic neurons. Phenotypical characterization and neuronal features of these cells have been described elsewhere (Gentile et al., 2012). A1 was plated in MEM/F12 (Gibco-BRL, Milan, Italy), supplemented with 10% FBS (Invitrogen, USA) medium. When cells reached 70% of confluence, were treated with Aβ1-42, AβpE3-42, or the peptides mixtures (5%, 33%, 50%) at a final concentration of 1 μM. The peptides and the mixtures were aggregated for 24 h at 37 °C at the concentration of 10 μM before dilution into culture media.

Cell viability determination A1 neuron cultures − After 48 h cells were harvested by trypsin-EDTA and the cell suspension diluted 1:10 in sterile PBS and mixed with equal volume of 0.4% Trypan Blue solution to evaluate cell viability. The ratio of live/dead cells was evaluated using an automated cell counter (TC20Bio-Rad Laboratories, Inc., Hercules, CA), as reported (Villa et al., 2016). Data were obtained by three independent experiments performed in quadrupli-

cate. Statistical analysis was performed by means of one-way ANOVA using "Newman-Keuls multiple comparison post-hoc test".

2.5. Turbidity

Aggregation kinetics were studied over time by monitoring the increase in turbidity at 37 °C. A small amount of concentrated Aβ peptides was injected into 0.5 cm path length quartz cuvette and mixed with PBS (150 mM, pH 7.4) to reach the concentration of 10 μM. Turbidity was determined measuring the absorbance at 405 nm, 3 times for each point, using a spectrophotometer Shimadzu UV-2700.

2.6. Circular dichroism (CD)

All samples were placed into 0.5 cm path length quartz cuvettes at the concentration of 10 μM; the spectra from 200 to 250 nm at 37 °C were obtained using a Jasco J-500A spectropolarimeter equipped with a Jasco IF-500-2 data processor. The spectropolarimeter was calibrated with an aqueous solution of (1S)-(+)-10-camphor sulfonic acid at 290.5 nm. The spectrum at each time was obtained by averaging three scans from 200 to 250 nm at a rate of 20 nm min^{-1} with a step resolution of 0.2 nm, a time constant of 4 s and a bandwidth of 2.0 nm. All the spectra were corrected by subtracting the PBS background. Deconvolution of the resulting spectra for the secondary structure estimation, was achieved using β-structure selection (BeStSel) algorithm by Micsonai et al. (2015).

2.7. NanoIR spectroscopy-spatially resolved IR imaging and spectra acquisition

For each measure, a 5 μl droplet of 10 μM pure or mixed Aβ peptides was deposited at the surface of an attenuated total internal reflection prism of ZnSe monocrystals and dried by means of a vacuum pump. Samples were scanned by a commercial nano-IR microscopy system (Anasys Instruments, Santa Barbara, USA) and with a line rate between 0.02-0.1 Hz in contact mode. We used a silicon cantilever (AppNano) with a nominal radius of 10 nm and a nominal spring constant of 0.5 N/m. All images have a resolution between 512×512 and 2048×2048 pixels. Height and IR amplitude images were first order flattened by SPIP (Image Metrology) software. Spectra were collected with a sampling of 2 cm^{-1} and with 256–2048 co-averages, within the range 1200–1800 cm^{-1} and with a spectral resolution of 8 cm^{-1}. Spectra were averaged (from at least 5 scans on the same position) and normalized by means of the microscope built-in Anasys software (Analysis Studio). Spectra were smoothed by means of a Savitzky-Golay filter in order to be compared (2nd order, 9 points).

2.8. Atomic force microscopy (AFM)

Analysis by AFM was performed on positively functionalized mica. After the cleaving, the substrate was incubated with a 10 μl drop of 0.05% (v/v) APTES ((3-Aminopropyl) triethoxysilane, Fluka) in Milli-Q water for 1 min at 20 °C, rinsed with Milli-Q water and then dried by a gentle flow of gaseous nitrogen. AFM samples preparation was realized at 20 °C by deposition of 10 μl of the 10 μM Aβ samples on the surface for 10 min. AFM images were made by means of a Park NX10 operating in tapping mode and equipped with a silicon tip (Nanosensor, SSS-NCHR, 40 Nm^{-1}) with a nominal apex radius of 3 nm. Images resolution is at least of 512×512 pixels. Images flattening and analysis was performed by SPIP (Image Metrology) software.

2.9. Transmission electron microscopy (TEM)

To evaluate dimensions of the aggregates in the peptides and their mixtures, 5 μl of 10 μM each Aβ sample were adsorbed for 10 min onto carbon coated 300-mesh copper grids. The samples were washed with 5 μl of Milli-Q water for 5 min, fixed for 3 min with 5 μl of 1% glutaraldehyde, and then negatively stained for 3 min with 5 μl of 2% Phosphotungstic Acid previously corrected to pH 7.2 with KOH 1 M. All air-dried specimens were examined with a Zeiss LEO 900 electron microscope (Zeiss, Stuttgart, Germany) operating at 80 kV. Images flattening and analysis was performed by ImageJ software.

3. Results

3.1. AβpE3-42 content, within the AβpE3-42/Aβ1-42 mixtures, induces different intracellular Ca^{2+} increase in cerebellar neurons

Disruption of intracellular Ca^{2+} homeostasis is among the earliest biochemical alterations induced by the interaction of amyloid aggregates with the cell membranes. Effects of Aβ peptides and mixtures long term exposure on intracellular free Ca^{2+} concentrations were measured in neurons by means of the fluorescent probe Oregon Green.

As reported in Fig. 1A, all Aβ peptides and mixtures were effective in increasing intracellular free Ca^{2+} concentration, although with different efficiency. As compared to Aβ1-42 alone, no significant changes in the Ca^{2+} response were observed for all mixtures and AβpE3-42 alone, with the exception of the 5% mixture, which induced a statistically significant increase (+147%).

3.2. Cell viability determination

Neuronal death by Aβ is considered as a direct consequence of altered Ca^{2+} homeostasis. To support the cellular changes seen on Ca^{2+} homeostasis, we evaluated A1 neuron survival in the presence of peptides alone and some mixtures (5%, 33% and 50%) at 1 μM. Quantification of cell death performed by Trypan Blue exclusion test, did not reveal significant differences between the A1 incubated with the peptides alone and the 33 and 50% mixtures, again with the exception of the 5% mixture showing its higher toxicity (Fig. 1B).

3.3. Conformational analysis

The secondary structures of the peptides alone and their mixtures, analyzed by CD, are reported in Fig. 2. We made the analysis of the secondary structure using β-structure selection (BeStSel) algorithm (Micsonai et al., 2015). In Table 1, the frequencies of secondary structures obtained from the BeStSel deconvolution of the CD spectra in Fig. 2, are reported. To highlight the quantitative differences between parallel and antiparallel β-sheet conformations we show the percentages of these structures with the histograms in Fig. 3A. The quantity of antiparallel β-sheet conformations increases along with the amount of pyroglutamylate peptide in the mixtures. Parallel β-sheet conformation instead, is high for Aβ1-42 alone (24%) and for the 2.5% mixture, while is zero for the 50% mixture and for AβpE3-42 alone.

As far as the turn conformation (Fig. 3B) Aβ1-42 alone displays the lowest percentage while AβpE3-42 alone and the 50% mixture have the highest frequencies. Other mixtures have intermediate per-
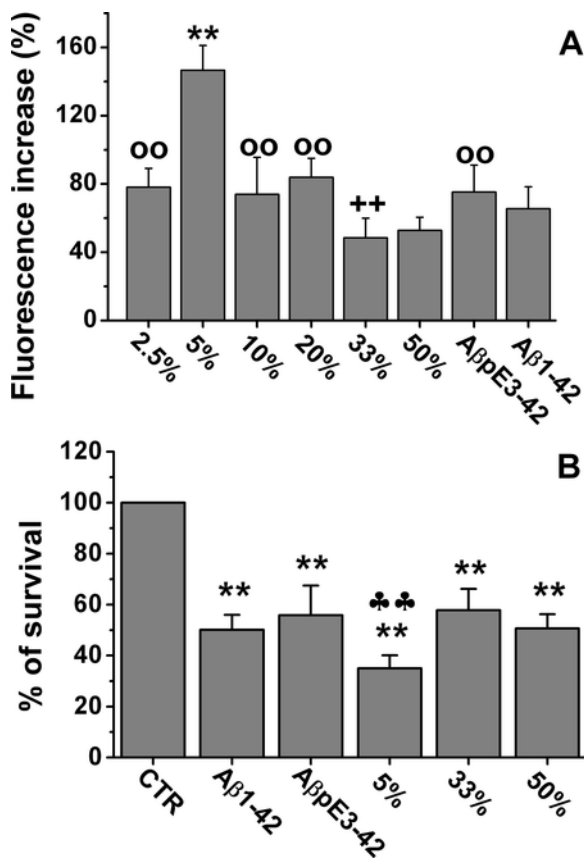
Fig. 1. Biological activity of different Aβ peptides and mixtures. All samples were aggregated for 24 h at 37 °C with total peptide concentration of 10 μM before dilution into culture media at 1 μM. A) Dysregulation of intracellular Ca^{2+} revealed by fluorescence microscopy. Neurons were treated with 1 μM of aggregates for 20 h at 37 °C. Oregon green probe was used at 6 μM. Fluorescence variation in percentage respect to the control. On x-axis are reported the samples. Mean ± standard error of the mean (s.e.m.), based on 2 replicates from 3 independent experiments. **p < 0.001 vs. 50%, 33% and Aβ1-42. ^{OO}p < 0.01 vs. 5%. $^{++}$p < 0.1 vs. 20%. B) A1 neuron cell viability. Viable cell number was assessed after 48 h of the Aβ addition. Data are expressed as percentage of vehicle-treated samples; each point represents the average of three experiments in quadruplicate. **p < 0.001 vs. vehicle-treated control values (CTR); $^{♣♣}$p < 0.05 vs. all the other Aβ peptides and mixtures treatment.
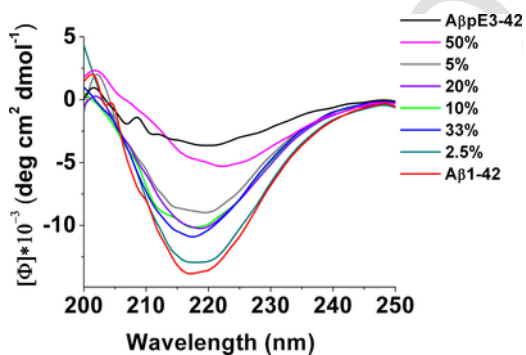

Fig. 2. CD spectra of the peptides alone and their mixtures after 24 h of incubation at 37 °C in PBS (pH 7,4), acquired between 200 and 250 nm. The total peptide concentration for all samples is 10 μM. CD results are expressed as Molar Ellipticity (deg cm^2 dmol^{-1}). The data shown are representative of those obtained in each independent experiment.

centages, weakly decreasing from 2.5% to 33%. If we assume that in an ideal mixture of a given composition there are not interactions between the Aβ1-42 and AβpE3-42 species, we can calculate its ideal CD spectrum as the weighted sum of the experimental signals of the two pure peptides in the corresponding mixture ratios. If in the mixtures there were interactions between the different species, the resulting spectrum should be different from the ideal spectrum. In Fig. 4 we report the comparison between the ideal and experimental CD spectra for two mixtures (33% and 50%), after 24 h of aggregation. The results of the comparison are very different in both cases (see Fig. 4, panels A and B). Comparing the peaks at 218 nm, corresponding to β-structure, we find that the 33% mixture displays a ratio between the experimental and ideal peak around the unit (1.11), suggesting the two peptides aggregate independently of one another. The minimal ratio, around 0.2, is obtained for the 50% mixture. The ratios for the other mixtures are between 0.7 and 0.9 (Table 2). Therefore in all the mixtures, except the 33%, the real aggregates have different β-conformation content in comparison to that calculated from the ideal spectra, showing that the interaction between the two peptides is important and has a great influence on the aggregation process.

Taking into account that the total β-structure content of each mixture is similar in all the mixtures, ranging between 47 and 52% from BeStSel algorithm, the differences between the experimental and ideal spectra should be in the specific components of the β-sheet structure. According to the BeStSel, β-sheet conformation consists of antiparallel β-sheet (left twisted, relaxed, right-twisted), parallel β-sheet and β-turn. We investigated which of these β-components gives a ratio, as a function of the percentage of AβpE3-42 in the mixtures, similar to the ratio between the experimental and ideal CD peaks at 218 nm. More specifically, the above ratio R is given by the equation:

$$R = E/I \tag{1}$$

where E is the BeStSel frequency of each type of β-component from the experimental spectrum and I the corresponding ideal frequency. I is calculated as:

$$I = [(\text{frequency of Aβ1-42 from BeStSel* fraction of Aβ1-42} \\ \text{in the analyzed mixture}) + (\text{frequency of AβpE3-42 from} \\ \text{BeStSel* fraction of AβpE3-42 in the analyzed mixture})] \tag{2}$$

As an example, for the 5% mixture the ideal value I of the parallel β-sheet structure, is calculated from Table 1 as I = [(24.3*0.95) + (0*0.05)] = 22.61, while the experimental value E is given in Table 1 as 12 to obtain R = 12/22.61 = 0.53.

The results are reported in Table 2, they show that the ratio between the experimental value and the ideal value of the parallel β-sheet structure follows the same profile of the ratio between the experimental and ideal values of the peaks at 218 nm. Indeed, we have the higher ratio (1.11) and lower ratio (0) for the 33% and 50% mixtures, respectively. Therefore, we can affirm that the parallel β-sheet content is related to the conformational change and then to the rate of the aggregation process, more than other β components (antiparallel β-sheet and β-turn).

3.4. Infrared nanospectroscopy

The secondary structure of the two peptides alone and the 5% mixture was also analyzed by Infrared nanospectroscopy (NanoIR) (Jackson and Mantsch, 1995; Zandomeneghi et al., 2004; Kong and Yu, 2007). This technique investigates not only the soluble but also

Table 1
The percentages of Secondary structure composition were estimated by BestSel algorithm after 24 h of incubation at 37 °C, 10 μM of total peptide concentration. RMSD = Root Mean Square Deviation represents the sample standard deviation of the differencies between the experimental and the estimated CD spectra.

| Sample	α −Helix (%)		β-Antiparallel (%)			β-Parallel (%)	Turn (%)	Others (%)	RMSD
	Regular	Distorted	Left twisted	Relaxed	Right twisted				
2.5%	0	0	0.6	8.1	8.1	17.7	13.0	52.5	0.1408
5%	0	1.2	4.3	17.8	2.9	11.7	10.5	51.6	0.1358
10%	0	0	0	14.3	8.1	15.8	11.4	50.3	0.1214
20%	0	0.5	0	14.7	13.6	14.8	9.5	46.9	0.1449
33%	5.2	1.9	4.7	9.0	18.4	16.0	8.3	36.5	0.2073
50%	0	2.4	5.8	11.7	13.9	0	15.9	50.2	0.2266
AβpE3-42	3.7	2.3	7.0	14.9	16.6	0	14.6	40.8	0.1560
Aβ1-42	0	0.5	0	12.2	14.5	24.3	5.7	42.7	0.0242
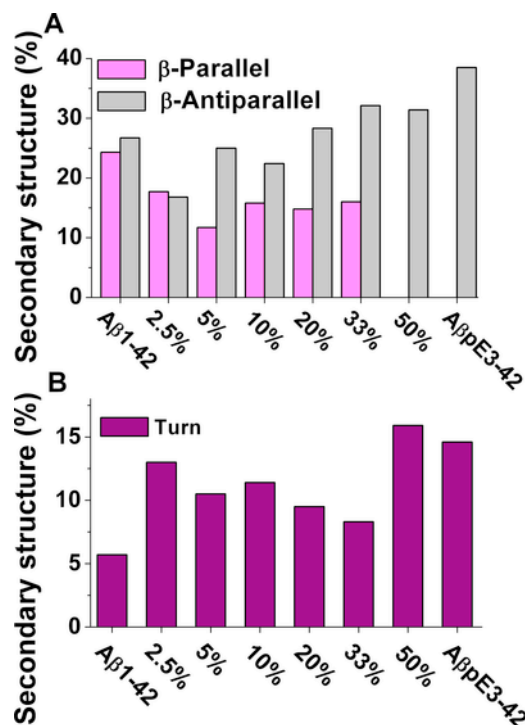
Fig. 3. Percentage of β-structures components determined by BeStSel software deconvolution of CD spectra acquired after 24 h of incubation at 37 °C in PBS (pH 7.4) with the total peptide concentration of 10 μM. A) β-parallel and β-antiparallel secondary structure for all samples; B) β-turn secondary structure for all samples.
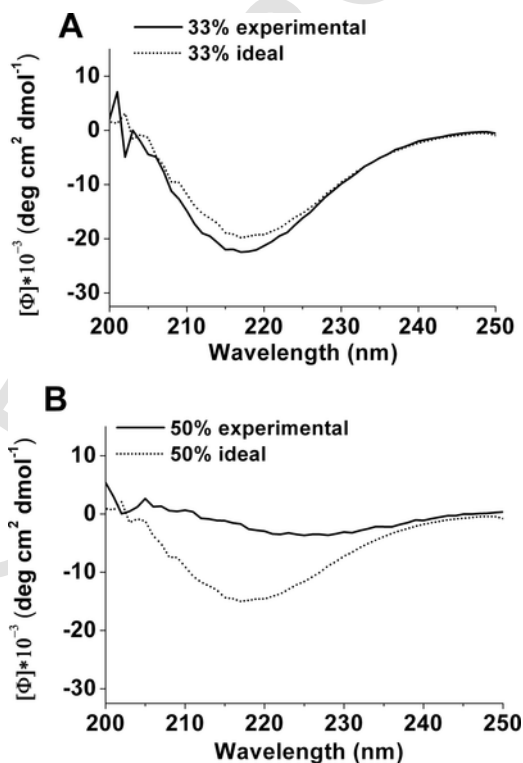

Fig. 4. Comparison of ideal and experimental CD spectra after 24 h of aggregation at 37 °C. The ideal spectra were calculated with the Eq. (1) in Section 3.3. A) 33% mixture. B) 50% mixture.

the precipitated aggregates. Each IR spectrum is obtained by averaging at least 10 spectra in the area of interest, which is indicated approximately by a full color circle in Fig. 5 Fig. 5 panel A, Fig. 6 panel A and B, and Fig. 7 panel A and B. In particular, the spectral shape of Amide I band allows to investigate the secondary structure content of the amyloidogenic species, (Calero and Gasset, 2012; Kumosinski and Unruh, 1996) while the second derivative of the spectrum resolves the contributions to the peak showing two main components in the Amide I band of all four aggregates. Aβ1-42 shows aggregates with a uniform composition (Fig. 5 panel A), where amyloid β-sheet (1623 cm^{-1}) and α-helix (1658 cm^{-1}) conformations dominate its secondary structure (Fig. 5 panel B and C). The unmodified peptide exhibits a β-sheet parallel, as confirmed by the absence of any shoulder between 1690 and 1700 cm^{-1}, which is typical of anti-parallel β-sheet. In the 5% mixture the presence of the pyroglutamylated peptide results in an increase of the structural heterogeneity of the sample

(Fig. 6 panel A and B). Furthermore, the sample presents the previous conformation with the addition of two shoulders, one at 1692 cm^{-1} related to antiparallel β-sheet content and the other at 1638 cm^{-1}, related to random coil conformation. AβpE3-42 alone (Fig. 7) shows a high β-sheet content (1623 cm^{-1}) and poor α-helix content (1658 cm^{-1}). In addition, we observe a small shoulder at 1638 cm^{-1}, related to the presence of random coil, between 1684 and 1695 cm^{-1}, related to β-turn and antiparallel β-sheet content.

3.5. Turbidity assay

When the β-amyloid peptide samples become insoluble, the turbidity of solution increases. The results after 24 and 100 h of incubation for all the samples are reported in Fig. 8. The turbidity after 24 h is very large for 50% and 5% mixtures and very small for 33% and

Table 2
Ratio between experimental and calculated peaks at 218 nm from CD spectra, R = E/I where E = value of the β structure component obtained from BeStSel for each mixture from the experimental spectra, I = [(frequency of Aβ1-42 from BeStSel * % of Aβ1-42 in the mixture analyzed) + (frequency of AβpE3-42 from BeStSel * % of AβpE3-42 in the mixture analyzed)], after 24 h of incubation at 37 °C.

Mixture	Ratio of peaks at 218 nm	Ratio of Parallel β-sheet	Ratio of Antiparallel β sheet			Ratio of Turn β-sheet
			left-twisted	relaxed	right-twisted	
2.5%	0.79	0.75	3.33	0.66	0.56	2.19
5%	0.67	0.53	12.28	1.44	0.20	1.71
10%	0.75	0.72	0	1.15	0.55	1.73
20%	0.87	0.76	0	1.15	0.91	1.27
33%	1.11	1.11	2.03	0.69	1.22	0.97
50%	0.17	0	1.65	0.86	0.89	1.57

20% mixtures. Turbidity increase from 24 to 100 h is different for each sample, indicating the formation of aggregates different in size and concentration. In the 33% mixture and in Aβ1-42 turbidity remains rather constant from 24 to 100 h, indicating that there is no more precipitation until the end of the experiment. The turbidity after 100 h from the 2.5% to the 20% mixtures is similar to that of AβpE3-42, even though slowly decreasing. The highest value of sedimentation after 100 h is that of the 50% mixture. Globally, turbidity experiments give the indication that just a minimal percentage of AβpE3-42, as 2.5 or 5%, has a big influence on the aggregation process of Aβ1-42.

3.6. AFM

In Fig. 9, we can observe 3-D morphology maps of all the mixtures samples and the peptides alone. Aβ1-42 shows typical amyloid fibrils with a length and height in the order of a 1 μm or less ad 6 nm, respectively. The 2.5% mixture shows fibrillar aggregates with similar morphology. The 5% mixture shows a higher degree of heterogeneity
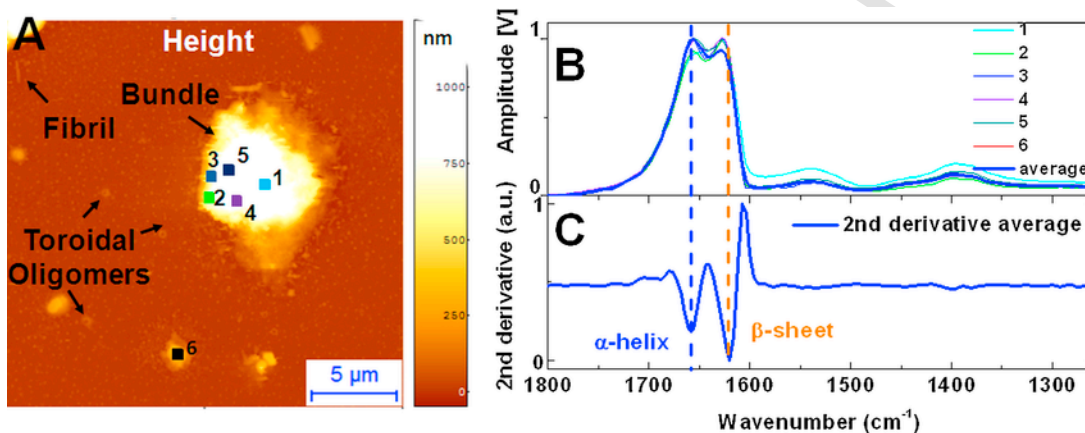
Fig. 5. Infrared nanospectroscopy of Aβ1-42 aggregates. A) AFM morphology map. B) FTIRspectra with average and C) 2nd derivative of the average spectra. All the aggregates were analysed after 24 h of incubation at 37 °C with a total peptide concentration of 10 μM. The position where each spectrum was acquired is indicated by a colored and numbered full circle in A).
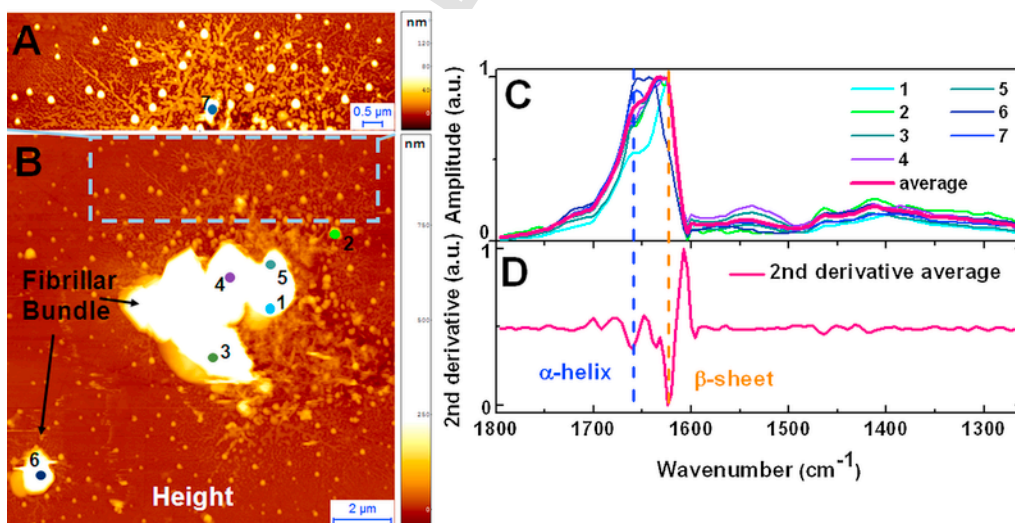
Fig. 6. Infrared nanospectroscopy of 5% AβpE3-42 in the mixture with Aβ1-42. A), B) AFM morphology map and detail of prefibrillar aggregates. C) FTIR spectra with average and D) 2nd derivative of the average spectra. All the aggregates were analysed after 24 h of incubation at 37 °C with a total peptide concentration of 10 μM. The position where the spectrum was acquired is indicated by a colored and numbered full circle in A) and B).
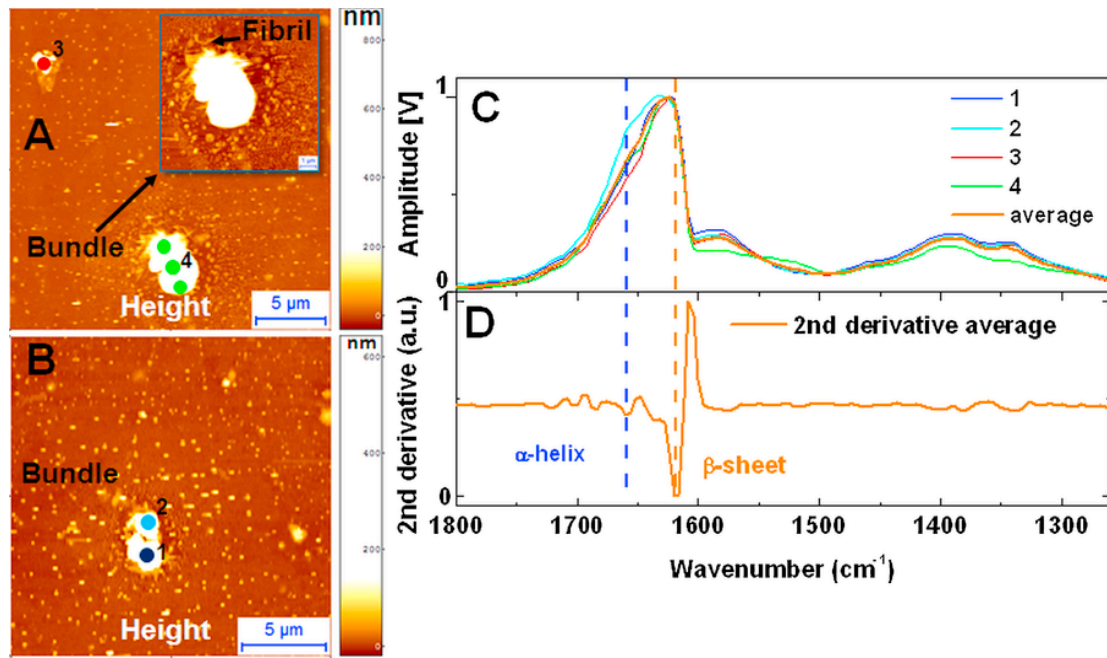
Fig. 7. Infrared nanospectroscopy of AβpE3-42 aggregates. A), B) AFM morphology map and detail of prefibrillar aggregates. C) FTIR spectra with average and D) 2nd derivative of the average spectra. All the aggregates were analysed after 24 h of incubation at 37 °C with a total peptide concentration of 10 μM. The position where the spectrum was acquired is indicated by a colored and numbered full circle in A) and B).
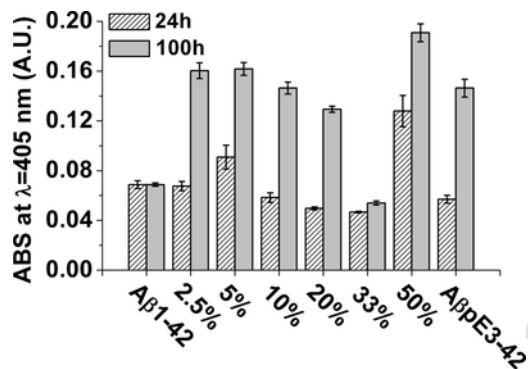

Fig. 8. Turbidity of the peptides alone and their mixtures after 24 and 100 h of aggregation at 37 °C in PBS (pH 7.4). The total peptide concentration for all samples is 10 μM. Results are expressed as absorbance at 405 nm. Mean ± s.e.m. based on 3 replicates from 2 independent experiments.

in morphology when compared to unmodified peptide and the other mixtures. In this sample, we could observe the coexistence of a population of short mature fibrils (data not shown) with a population of abundant spheroidal aggregates of various diameters, starting in the order of 1 nm up to hundreds of nanometer. The 10% and 20% mixtures contain longer and entangled mature fibrils (i.e. height in the order of 6 nm). While, in the 33 and 50% mixtures, the fibril interactions increase with the pyroglutamylated peptide content, forming large aggregates that start resembling amorphous aggregates as in the case of AβpE3-42 alone.

3.7. TEM

In Fig. 10 panel A, the morphology of Aβ1-42 is reported, showing typical amyloid fibrils, with dimensions lower than for the other samples. This result can be explained remembering that this peptide

has slow aggregation kinetics and therefore its typical long fibrils still have to grow after 24 h of incubation (Table 3). In other micrographs of the full length peptide (data not shown) also small spheroidal aggregates with a diameter around 20 nm (Table 3) are displayed. In Fig. 10 panels B–H, the morphology of the 2.5%, 5%, 10%, 20%, 33%, 50% mixtures and AβpE3-42, respectively, are shown. These samples are characterized by long entangled fibrils and small spheroidal aggregates with different dimensions, reported in Table 3. The micrograph of the 5% sample shows a different morphology than the other mixtures and peptides alone, indeed we can observe the presence of big spheroidal aggregates and few short fibrils (Table 3).

4. Discussion

In this study we tested different ratios of AβpE3-42 in the mixture with Aβ1-42 and we found a correlation between the biological activity, the structure and morphology of the analyzed mixtures. In order to compare easily the biophysical changes at each ratio of peptides, we report a summary of the main results from our experiments in Table 4. The most striking difference is between the mixtures from the 2.5% to the 33% and the 50% mixture: in the first group of mixtures, there are parallel β-sheet conformations, completely absent in the second as in AβpE3-42 alone. β-turn conformation and the turbidity assay confirm the different behavior of the mixtures below the 33% compared to the 50% mixture. Comparable results are found looking at the ratio (R) between experimental and ideal CD peaks at 218 nm. We conclude that AβpE3-42 causes template-induced misfolding of Aβ1-42 at concentrations below 33%, this effect is high at low concentration of the truncated peptide (2.5 and 5%) and it decreases until the concentration of 33% of AβpE3-42, which we define as the critical concentration to have seeded aggregation of Aβ1-42.

The structural impact of pyroglutamylate on Aβ1-42 up to the 33% is indicative of a prion-like effect, because below this concentration, AβpE3-42 is not able to interact with itself and so it is forced to
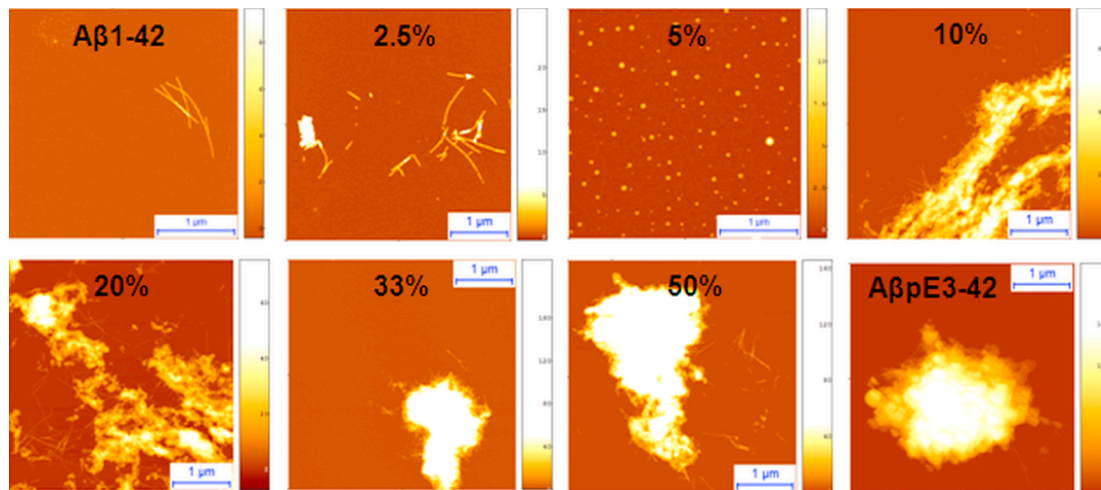
Fig. 9. Morphology by AFM. All the aggregates were analyzed after 24 h of incubation at 37 °C with a total peptide concentration of 10 μM.
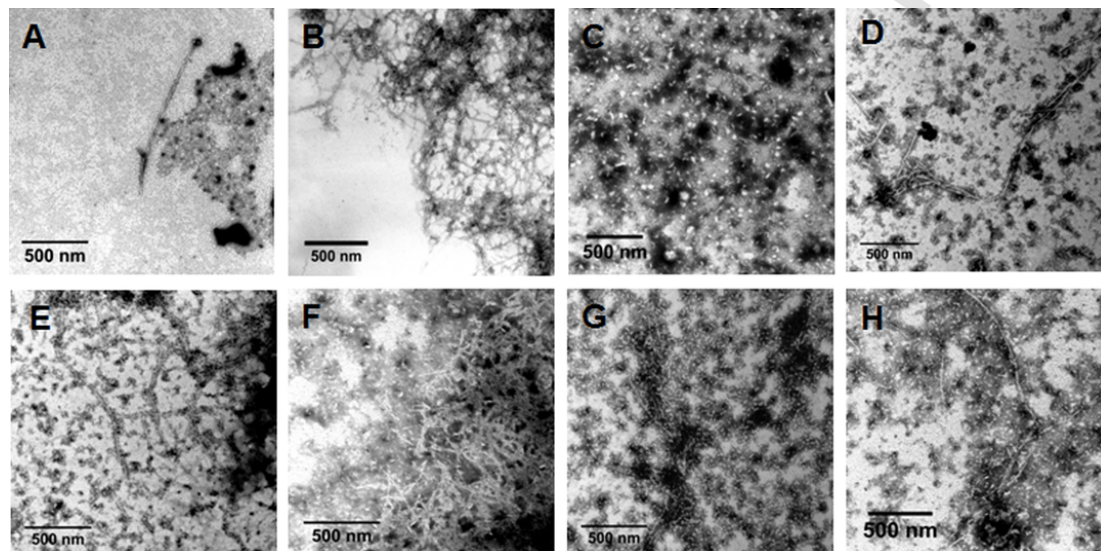

Fig. 10. Morphology by TEM. All the aggregates were analyzed after 24 h of incubation at 37 °C with a total peptide concentration of 10 μM. A) Aβ1-42; B) 2.5% mixture; C) 5% mixture; D) 10% mixture; E) 20% mixture; F) 33% mixture; G) 50% mixture; H) AβpE3-42.

Table 3
Dimensions of aggregates from TEM micrographs after 24 h of aggregation at 37 °C. SE = Standard error of the mean.

Sample	Spheroid Diameter (nm) ± SE	N total	Fibril Length (nm) ± SE	N total
Aβ1-42	20.70 ± 0.06	80	220 ± 5	84
2.5% mixture	29.90 ± 0.15	61	562 ± 45	11
5% mixture	40.20 ± 0.04	360	331 ± 10	23
10% mixture	28.10 ± 0.10	111	533 ± 29	14
20% mixture	25.60 ± 0.05	129	829 ± 87	5
33% mixture	26.30 ± 0.06	108	592 ± 54	8
50% mixture	26.90 ± 0.04	156	465 ± 47	5
AβpE3-42	25.00 ± 0.04	165	646 ± 7	46

aggregate with the other peptide modifying its structure (Matos et al., 2014). On the contrary, when it is at high concentration (50%), the seed effect is not more possible because AβpE3-42 self-aggregates and, been faster than Aβ1-42, controls the total aggregation kinetics.

The measurement of the biological activity shows that intraneuronal free Ca^{2+} is maximum for the mixture containing 5% of AβpE3-42. This result is supported by the cell viability determination where the 5% mixture confirms its high toxicity. These data are in agreement with previous reports by Nussbaum et al. (2012) that found a marked enhancement of Aβ1-42 toxicity in the 5% mixture, with formation of metastable LNOs that are more cytotoxic to neurons than those made from Aβ1-42 alone. Furthermore, the 5% mixture shows the highest content in relaxed antiparallel β-sheet, indicating a deep correlation between the biological activity and the biophysical properties of the aggregates. The presence of the antiparallel β-sheet in the 5% mixture is also confirmed by the NanoIR experiments. Notably, in literature is reported that the antiparallel β-structure is related to the toxic properties of oligomeric structures (Cerf et al., 2009; Celej et al., 2012) thus allowing us to correlate well this result with the biological activity. In addition, between the mixtures with a low content of AβpE3-42, the 5% mixture shows a low content for parallel β-sheet, indicating that this mixture has a low tendency to fibrillization. This is confirmed by the morphology experi-

Table 4
Summary of the results from Tables 1–3. R = Relaxed; RT = Right-Twisted; //β-sheets = parallel β-sheets; anti//β-sheets = antiparallel β-sheets; SD = Spheroid Diameter; FL = Fibrils Length. The most relevant data are in bold and underlined.

Sample	Anti//β-sheet (%)		//β- sheets (%)	Turn (%)	Ratio of peaks at 218 nm	Ratio of //β-sheet	Ratio of Anti//β-sheet (%)		Dimensions from TEM	
	R	RT					R	RT	SD (nm)	FL (nm)
2.5%	8.1	8.1	17.7	13.0	0.79	0.75	0.66	0.56	29.9	562
5%	*17.8*	*2.9*	*11.7*	10.5	*0.67*	*0.53*	*1.44*	*0.20*	*40.2*	*331*
10%	14.3	8.1	15.8	11.4	0.75	0.72	1.15	0.55	28.1	533
20%	14.7	13.6	14.8	9.5	0.87	0.76	1.15	0.91	25.6	829
33%	9.0	18.4	*16.0*	*8.3*	*1.11*	*1.11*	0.69	1.22	26.3	592
50%	11.7	13.9	0	*15.9*	*0.17*	*0*	0.86	0.89	26.9	465
AβpE3-42	14.9	16.6	0	14.6					25.0	646
Aβ1-42	12.2	14.5	24.3	5.7					20.8	220

ments, that show spheroidal aggregates bigger than in other samples, and many separated fibrils, shorter than in other mixtures. A possible explanation is that in the 5% mixture, AβpE3-42 destabilizes the initial parallel β oligomers of Aβ1-42 to generate antiparallel β-relaxed oligomers thus delaying the fibril formation.

We suggest here that the big spheroidal aggregates, or the short fibrils, might insert in the lipid bilayer of cell membrane forming artificial pores and change the calcium homeostasis (Small et al., 2009), that have previously been implicated in Aβ toxicity (Gunn et al., 2016; Salahuddin et al., 2016) as confirmed in this paper. Besides, the spheroidal shape of these aggregates might interact with particular receptors (Supnet et al., 2006; Danysz and Parsons, 2012) or penetrate in the neurons and cause their death better than other types of aggregates.

The unique properties of the 5% mixture may correlate with the clinical outcome of low concentrations of AβpE3-x in the core of aggregates extracted from cerebral deposits from sporadic AD. AβpE3-x species are present in intra- and extracellular amyloid deposits, mainly in plaques with a dense core and always in the center of these aggregates (Perez-Garmendia et al., 2014). Other studies (Mandler et al., 2014) using monoclonal antibody, found in the early stages of AD a discrete amount of AβpE3-x aggregates, while in the later stages of AD, AβpE3-x species were abundant in diffuse and mature plaques, suggesting that the peri-synaptic accumulation of AβpE3-x peptides can contribute to the early cognitive dysfunction in AD. Depending on the method of detection, the relative amount of AβpE3-x Aβ in human brain was described between 1% as measured by ELISA (Schilling et al., 2008) and 27% as measured by mass spectrometry (Guntert et al., 2006). This was recently corroborated by detailed analysis of regional and temporal appearance of general Aβ and pGlu-3 Aβ in sporadic AD (Cynis et al., 2016).

5. Conclusions

In this paper, we validate that the pyroglutamylated peptide has a large influence on the structure and toxicity of the unmodified peptide especially at low AβpE3-42 content, by transmission of specific structural features to the unmodified peptide (Nussbaum et al., 2012; Matos et al., 2014). We suggest that, acting as seed of Aβ aggregation, pyroglutamylated peptides could be one of the fundamental actors initiating AD pathology onset. Studies on the interaction between these peptides by higher resolution methods such as NMR (work in progress), will lead to more detailed models of the structure and interaction of mixed aggregates. We believe that the comprehension of the structure of the toxic aggregates in AD is key to design therapies that prevent their formation and therefore the pathology.

Conflict of interest

The authors declare that they have no conflicts of interest with the contents of this article.

References

Brookmeyer, R., Gray, S., Kawas, C., 1998. Projections of Alzheimer's disease in the United States and the public health impact of delaying disease onset. Am. J. Public Health 88, 1337–1342.

Brookmeyer, R., Johnson, E., Ziegler-Graham, K., Arrighi, H.M., 2007. Forecasting the global burden of Alzheimer's disease. Alzheimers Dement. 3, 186–191.

Calero, M., Gasset, M., 2012. Featuring amyloids with Fourier transform infrared and circular dichroism spectroscopies. Methods Mol. Biol. 849, 53–68.

Celej, M.S., Sarroukh, R., Goormaghtigh, E., Fidelio, G.D., Ruysschaert, J.M., Raussens, V., 2012. Toxic prefibrillar α-synuclein amyloid oligomers adopt a distinctive antiparallel β-sheet structure. Biochem. J. 443, 719–726.

Cerf, E., Sarroukh, R., Tamamizu-Kato Breydo, L., Derclaye, S., Dufr, Y.F., 2009. Antiparallel β-sheet: a signature structure of the oligomeric amyloid β-peptide. Biochem. J. 421, 415–423.

Cynis, H., Frost, J.L., Helen Crehan, H., Lemere, C.A., 2016. Immunotherapy targeting pyroglutamate-3 Aβ: prospects and challenges. Mol. Neurodegener. 11, 48.

D'Arrigo, C., Tabaton, M., Perico, A., 2009. N-terminal truncated pyroglutamyl beta amyloid peptide Abetapy3-42 shows a faster aggregation kinetics than the full-length Abeta1-42. Biopolymers 91, 861–873.

Danysz, W., Parsons, C.G., 2012. Alzheimer's disease, beta-amyloid, glutamate, NMDA receptors and memantine-searching for the connections. Br. J. Pharmacol. 167, 324–352.

Frost, J.L., Le, K.X., Cynis, H., Kleinschmidt, M., Palmour, R.M., Ervin, F.R., Snigdha, S., Cotman, C.W., Saido, T.C., Vassar, R.J., St. George-Hyslop, P., Ikezu, T., Schilling, S., Demuth, H.U., Lemere, C.A., 2013. Pyroglutamate-3 amyloid-beta deposition in the brains of humans, non-human primates, canines, and Alzheimer disease-like transgenic mouse models. Am. J. Pathol. 183, 369–381.

Galante, D., Corsaro, A., Florio, T., Vella, S., Pagano, A., Sbrana, F., Vassalli, M., Perico, A., D'Arrigo, C., 2012. Differential toxicity, conformation and morphology of typical initial aggregation states of Abeta1-42 and Abetapy3-42 beta-amyloids. Int. J. Biochem. Cell. Biol. 44, 2085–2093.

Gentile, M.T., Nawa, Y., Lunardi, G., Florio, T., Matsui, H., Colucci- D'Amato, L., 2012. Tryptophan hydroxylase 2 (TPH2) in a neuronal cell line: modulation by cell differentiation and NRSF/rest activity. J. Neurochem. 123 (6), 963–970.

Gunn, A.P., Wong, B.X., Johanssen, T., Griffith, J.C., Masters, C.L., Bush, A.I., Barnham, K.J., Duce, J.A., Cherny, R.A., 2016. Amyloid-β peptide Aβ3pE-42 induces lipid peroxidation, membrane permeabilization, and calcium influx in neurons. J. Biol. Chem. 291 (12), 6134–6145.

Guntert, A., Dobeli, H., Bohrmann, B., 2006. High sensitivity analysis of amyloid-beta peptide composition in amyloid deposits from human and PS2APP mouse brain. Neuroscience 143, 461–475.

Hung, L.W., Ciccotosto, G.D., Giannakis, E., Tew, D.J., Perez, K., Masters, C.L., Cappai, R., Wade, J.D., Barnham, K.J., 2008. Amyloid-beta peptide (Abeta) neurotoxicity is modulated by the rate of peptide aggregation: abeta dimers and trimers correlate with neurotoxicity. J. Neurosci. 28, 11950–11958.

Jackson, M., Mantsch, H.H., 1995. The use and misuse of ftir spectroscopy in the determination of protein-structure. Crit. Rev. Biochem. Mol. Biol. 30, 95–120.

Jeong, J.S., Ansaloni, A., Mezzenga, R., Lashuel, H.A., Dietler, G., 2013. Novel mechanistic insight into the molecular basis of amyloid polymorphism and secondary nucleation during amyloid formation. J. Mol. Biol. 425, 1765–1781.

Kirkitadze, M.D., Bitan, G., Teplow, D.B., 2002. Paradigm shifts in Alzheimer's disease and other neurodegenerative disorders: the emerging role of oligomeric assemblies. J. Neurosci. Res. 69, 567–577.

Kong, J., Yu, S., 2007. Fourier transform infrared spectroscopic analysis of protein secondary structures. Acta Biochim. Biophys. Sin. 39, 549–559.

Kumosinski, T.F., Unruh, J.J., 1996. Quantitation of the global secondary structure of globular proteins by FTIR spectroscopy: comparison with X-ray crystallographic structure. Talanta 43, 199–219.

Levi, G., Aloisi, F., Ciotti, M.T., Gallo, V., 1984. Autoradiographic localization and depolarization-induced release of acidic amino acids in differentiating cerebellar granule cell cultures. Brain Res. 290, 77–86.

Mandler, M., Walker, L., Santic, R., Hanson, P., Upadhaya, A.R., Colloby, S.J., Morris, C.M., Thal, D.R., Thomas, A.J., Schneeberger, A., Attems, J., 2014. Pyroglutamylated amyloid-beta is associated with hyperphosphorylated tau and severity of Alzheimer's disease. Acta Neuropathol. 128, 67–79.

Matos, J.O., Goldblatt, G., Jeon, J., Chen, B., Tatulian, S.A., 2014. Pyroglutamylated amyloid-beta peptide reverses cross beta-sheets by a prion-like mechanism. J. Phys. Chem. B 118, 5637–5643.

Micsonai, A., Wien, F., Kernya, L., Lee, Y.H., Goto, Y., Refregiers, M., Kardos, J., 2015. Accurate secondary structure prediction and fold recognition for circular dichroism spectroscopy. PNAS 112, E30095–103.

Moore, B.D., Chakrabarty, P., Levites, Y., Kukar, T.L., Baine, A.M., Moroni, T., Ladd, T.B., Das, P., Dickson, D.W., Golde, T.E., 2012. Overlapping profiles of Abeta peptides in the Alzheimer's disease and pathological aging brains. Alzheimers Res. Ther. 4, 18.

Nussbaum, J.M., Schilling, S., Cynis, H., Silva, A., Swanson, E., Wangsanut, T., Tayler, K., Wiltgen, B., Hatami, A., Ronicke, R., Reymann, K., Hutter-Paier, B., Alexandru, A., Jagla, W., Graubner, S., Glabe, C.G., Demuth, H.U., Bloom, G.S., 2012. Prion-like behaviour and tau-dependent cytotoxicity of pyroglutamylated amyloid-beta. Nature 485, 651–655.

Pellistri, F., Bucciantini, M., Relini, A., Nosi, D., Gliozzi, A., Robello, M., Stefani, M., 2008. Nonspecific interaction of prefibrillar amyloid aggregates with glutamatergic receptors results in Ca^{2+} increase in primary neuronal cells. J. Biol. Chem. 283, 29950–29960.

Perez-Garmendia, R., Hernandez-Zimbron, L.F., Morales, M.A., Luna-Munoz, J., Mena, R., Nava Catorce, M., Acero, G., Vasilevko, V., Viramontes-Pintos, A., Cribbs, D.H., Gevorkian, G., 2014. Identification of N-terminally truncated pyroglutamate amyloid-beta in cholesterol-enriched diet-fed rabbit and AD brain. J. Alzheimers Dis. 39, 441–455.

Perico, A., Galante, D., D'Arrigo, C., 2011. Structure and toxicity of the prefibrillar aggregation states of beta peptides in alzheimer's disease. In: De La Monte, S. (Ed.), Alzheimer's Disease Pathogenesis-Core Concepts, Shifting Paradigms and Therapeutic Target. INTECH Book, pp. 157–172.

Petkova, A.T., Leapman, R.D., Guo, Z., Yau, W.M., Mattson, M.P., Tycko, R., 2005. Selfpropagating, molecular-level polymorphism in Alzheimer's beta-amyloid fibrils. Science 307, 262–265.

Pivtoraiko, V.N., Abrahamson, E.E., Leurgans, S.E., DeKosky, S.T., Mufson, E.J., Ikonomovic, M.D., 2015. Cortical pyroglutamate amyloid-β levels and cognitive decline in Alzheimer's disease. Neurobiol. Aging 36 (January (1)), 12–19.

Robello, M., Amico, C., Cupello, A., 1993. Regulation of GABAA receptor in cerebellar granule cells in culture: differential involvement of kinase activities. Neuroscience 53, 131–138.

Russo, C., Schettini, G., Saido, T.C., Hulette, C., Lippa, C., Lannfelt, L., Ghetti, B., Gambetti, P., Tabaton, M., Teller, J.K., 2000. Presenilin-1 mutations in Alzheimer's disease. Nature 405, 531–532.

Russo, C., Violani, E., Salis, S., Venezia, V., Dolcini, V., Damonte, G., Benatti, U., D'Arrigo, C., Patrone, E., Carlo, P., Schettini, G., 2002. Pyroglutamate-modified amyloid beta-peptides AbetaN3(pE) strongly affect cultured neuron and astrocyte survival. J. Neurochem. 82, 1480–1489.

Saido, T.C., Iwatsubo, T., Mann, D.M., Shimada, H., Ihara, Y., Kawashima, S., 1995. Dominant and differential deposition of distinct beta-amyloid peptide species, A beta N3(pE), in senile plaques. Neuron 14, 457–466.

Salahuddin, P., Fatima, M.T., Abdelhameed, A.S., Nusrat, S., Khan, R.H., 2016. Structure of amyloid oligomers and their mechanisms of toxicities: targeting amyloid oligomers using novel therapeutic approaches. Eur. J. Med. Chem. 114, 41–58.

Sanders, H.M., Lust, R., Teller, J.K., 2009. Amyloid-beta peptide Abetap 3–42 affects early aggregation of full-length Abeta1-42. Peptides 30, 849–854.

Schilling, S., Lauber, T., Schaupp, M., Manhart, S., Scheel, E., Bohm, G., Demuth, H.U., 2006. On the seeding and oligomerization of pGlu-amyloid peptides (in vitro). Biochemistry 45, 12393–12399.

Schilling, S., Zeitschel, U., Hoffmann, T., Heiser, U., Francke, M., Kehlen, A., Holzer, M., Hutter-Paier, B., Prokesch, M., Windisch, M., Jagla, W., Schlenzig, D., Lindner, C., Rudolph, T., Reuter, G., Cynis, H., Montag, D., Demuth, H.U., Rossner, S., 2008. Glutaminyl cyclase inhibition attenuates pyroglutamate Abeta and Alzheimer's disease-like pathology. Nat. Med. 14, 1106–1111.

Small, D.H., Gasperini, R., Vincent, A.J., Hung, A.C., Foa, L., 2009. The role of Aβ-Induced calcium dysregulation in the pathogenesis of alzheimer's disease. J. Alzheimers Dis. 16, 225–233.

Supnet, C., Grant, J., Kong, H., Westaway, D., Mayne, M., 2006. Amyloid-β_{1-42} increases ryanodine receptor-3 expression and function in neurons of TgCRND8 mice. J. Biol. Chem. 281, 38440–38447.

Tabaton, M., Nunzi, M.G., Xue, R., Usiak, M., Autilio-Gambetti, L., Gambetti, P., 1994. Soluble amyloid beta-protein is a marker of Alzheimer amyloid in brain but not in cerebrospinal fluid. Biochem. Biophys. Res. Commun. 200, 1598–1603.

Tanzi, R.E., 2005. The synaptic Abeta hypothesis of Alzheimer disease. Nat. Neurosci. 8, 977–979.

Upadhaya, A.R., Kosterin, I., Kumar, S., von Arnim, C.A.F., Yamaguchi, H., Fandrich Walter, M.J., Thal, D.R., 2014. Biochemical stages of amyloid-β peptide aggregation and accumulation in the human brain and their association with symptomatic and pathologically preclinical Alzheimer's disease. Brain 137, 887–903.

Villa, V., Thellung, S., Corsaro, A., Novelli, F., Tasso, B., Colucci-D'Amato, L., Gatta, E., Tonelli, M., Florio, T., 2016. Celecoxib inhibits prion protein 90–231 mediated pro-inflammatory responses in microglial cells. Mol. Neurobiol. 53, 57–72.

Walsh, D.M., Klyubin, I., Faddeeva, J.V., Cullen, W.K., Anwyl, R., Wolfe, M.S., Rowan, M.J., Selkoe, D.J., 2002. Naturally secreted oligomers of amyloid beta protein potently inhibit hippocampal long-term potentiation in vivo. Nature 416, 535–539.

Wu, G., Miller, R.A., Connolly, B., Marcus, J., Renger, J., Savage, M.J., 2014. Pyroglutamate-modified amyloid-beta protein demonstrates similar properties in an Alzheimer's disease familial mutant knock-in mouse and Alzheimer's disease brain. Neurodegener. Dis. 14 (2), 53–66.

Zandomeneghi, G., Krebs, M.R., McCammon, M.G., Fandrich, M., 2004. FTIR reveals structural differences between native beta-sheet proteins and amyloid fibrils. Protein Sci. 13, 3314–3321.